Renewable and Sustainable Energy Reviews 20 (2013) 142–154

Contents lists available at SciVerse ScienceDirect

Renewable and Sustainable Energy Reviews

journal homepage: www.elsevier.com/locate/rser

A review of optimized design layouts for solar power tower plants with *campo* code

Francisco J. Collado*, Jesús Guallar

Dpto. de Ingeniería Mecánica, EINA, Universidad de Zaragoza, María de Luna 3, 50018 Zaragoza, Spain

ARTICLE INFO

Article history:
Received 21 October 2012
Received in revised form
27 November 2012
Accepted 28 November 2012
Available online 28 December 2012

Keywords:
Solar tower power
Optimized heliostat layouts
Campo code

ABSTRACT

Solar power tower (SPT) systems are viewed as one of the most promising technologies for producing solar electricity, in which direct solar radiation is reflected and concentrated by a field of giant mirrors (heliostats) onto a receiver placed at the top of a tower. However, the optimized design of a heliostat field is a rather complex problem because the annual performance of a heliostat is a function of not only the instants of time considered and its own position, but also the relative location of neighbouring heliostats, which cause shadows and blockings. A variety of procedures may be found in the open literature, although there is great lack of information on the details of an optimized layout. This review shows that these complex problems have partially led to the expansion of parabolic trough technologies in USA and Spain in spite of their lower thermodynamic efficiencies compared with solar tower power. As a modest support of SPT systems, the authors have presented elsewhere the abilities of a new code called *campo* for fast and accurate calculations of the shadowing and blocking factor for each and every heliostat. This work explores a review of the optimized heliostat field layouts yielded by *campo. Campo* commences the optimization search based on the densest layout, with the worst shadowing and blocking factor, but with good values for the other optical factors, and then progresses towards gradually expanded distributions. The search for maximum annual energy through *campo* results in a clear, steady and reproducible procedure. Finally, as an example of this new procedure, some options of optimized heliostat field layouts are reviewed using as input parameters the scarce open literature data on *Gemasolar*, the first solar power tower commercial plant with molten salt storage in the world.

Contents

* Corresponding author. Tel.: +34 976 762551; fax: +34 976 762616.
E-mail address: fjk@unizar.es (F.J. Collado).

1364-0321 © 2012 Elsevier Ltd. Open access under CC BY-NC-ND license.
http://dx.doi.org/10.1016/j.rser.2012.11.076

1. Introduction

Among the renewable technologies available for large-scale power production today and for the next few decades, concentrating solar thermal power (CSP) is one with the potential to make major clean energy contributions because of its relatively conventional technology and ease of scale-up [1–6].

Solar power tower (SPT) systems, in which direct solar radiation is focused onto a receiver mounted on top of a tower by means of a field of two-axis tracking heliostats (giant mirrors), are known to be one of the most promising CSP technologies for producing solar electricity in the mid-load power range (≥ 50 MWe) [1–2]. SPT systems have already proved their ability to generate clean electricity in the 20 MWe size in Spain [7], while a 100-MWe SPT plant is under construction in USA [8].

SPT plants are currently competing with parabolic trough systems (PT) to generate clean power (more details about the PT technology can be found in [6]). Both systems are experiencing a major boost in their expansion and size. As we will see later in a review of the development and current status of these technologies, SPT and PT plants of about 300 MWe are expected in future years in USA [9].

This paper is centred on the optimized design procedures of heliostat field layouts in SPT systems in a modest attempt to make the designs of heliostat fields less complex. The current battle of SPT systems against PT technologies requires R&D support in the design, development, and testing of larger receivers, larger heliostats, and larger fields to reduce scale-up risk [1–3]. The need for new tools to scale-up SPT systems is also highlighted by DOE [10]: as the size of the SPT increases, the optical efficiency (the ratio of sunlight capture to incident sunlight) declines. Thus system re-optimization is required.

The heliostat field, the main focus of this study, is the key subsystem in solar power towers because it typically contributes about 50% [11] to the total cost of the plant and results in power losses of 40% [1]. Furthermore, the DLR ECOSTAR study [2] also concludes that innovation potentials with the highest impact on SPT-cost reduction are increases in heliostat size and plant scale (≥ 50 MWe). In view of current and near-future trends in USA [9], this increase in plant scale is already underway.

Clearly, any heliostat field optimization should be based on a fast and accurate calculation of the optical efficiency of a heliostat. Following classic Sandia nomenclature [12], which has also been used by the authors in former works [13,14], the instantaneous optical efficiency of a heliostat η is

$$\eta(x,y,t) = \rho \cos\omega(x,y,t)\ f_{\mathrm{at}}(x,y)\ f_{\mathrm{int}}(x,y,t)\ f_{\mathrm{sb}}(x,y,t,\text{neighbour heliostats}), \quad (1)$$

where ρ is the actual mirror reflectivity, $\cos\omega$ the cosine of the incidence angle between the sun rays and the heliostat normal, f_{at} the atmospheric attenuation factor, f_{int} the intercept factor, i.e., the fraction of the energy spot reflected by the heliostat hitting onto the receiver surface, and finally f_{sb} is the shadowing (of incident sunlight by adjacent heliostats) and blocking (of reflected sunlight by neighbouring mirrors) factor, i.e., the fraction of the heliostat area free from shadowing and blocking, see Fig. 1.

The relation of this efficiency η with energy is immediate. The instantaneous power P_m (kW/m^2-mirror) sent by any heliostat onto the receiver will be

$$P_m(x,y,t) = \eta(x,y,t)\ I_D(t) \quad (2)$$

where I_D (kW/m^2) is the instantaneous normal direct solar intensity for the chosen location and time t.

Notice that, in general, the denser the heliostats in the field, the worse the shadowing and blocking factor and better the other optical factors in Eq. (1). This is the shadowing and blocking-heliostat density trade-off, which has been well-known since the pioneering works of Houston University [15–17].

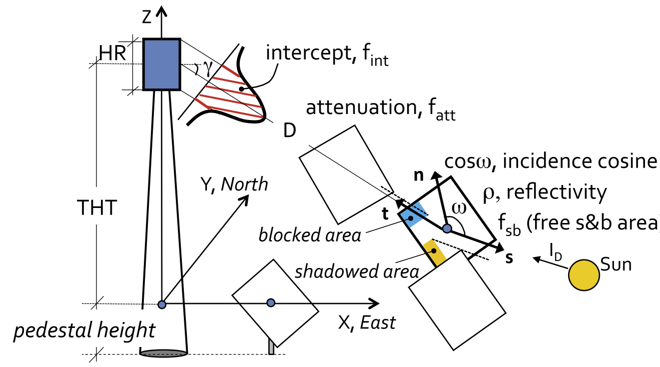


Fig. 1. Nomenclature of optical efficiency in heliostat fields.

However, in view of Eq. (1), the optimized design of heliostat fields in SPT plants is a rather complex problem for two reasons.

First, the instantaneous energy sent by a single heliostat, see Eq. (1), depends not only on its own location in the field and the instant of time considered, but also on the relative position of neighbouring heliostats that may cause shading and/or blocking onto it. This issue has been recently treated in depth by the authors elsewhere [14], in which a new code called *campo*, for the optimized design of heliostat fields, was presented.

Second, the figure of merit in the full optimization process of the collector field is usually the capital cost divided by the annual energy reaching the receiver [15–20]. This annual energy is the sum of the instantaneous energy, see Eqs. (1) and (2), produced by the whole field (there may be thousands of heliostats) along the instants of time (tens) sampled in a typical meteorological year (TMY). Concerning the capital cost, only companies with the capacity to design and construct an SPT system will know, obviously, as this is proprietary information, the accurate costs of the various elements in the collector field although some estimates can be found in [1,11].

Given the complexity of the problem and the expensive computation times, rather different codes with their specific simplifications may be found in the open literature. In [21], Garcia et al. present a general review of the most used codes (published by 2008), and divide the available codes into two categories defined by the calculation procedure for the spillage factor and shadings and blockings, see Eq. (1). MIRVAL [22] and SolTRACE [23] (the latter is free to download at [24]) are typical codes based on Monte Carlo ray-tracing, whereas University of Houston-RCELL [15–17], DELSOL3 (recently winDELSOL) from Sandia Labs [18] and HFLCAL from the German Aerospace Centre (DLR) [19,20] calculate the energy spot sent by a heliostat (and therefore the spillage) through the convolution of various error cones associated with rays reflected from the mirrors. Furthermore, these convolution codes usually calculate the shadowing and blocking factor projecting the outlines of the neighbouring heliostats onto the plane of the analyzed heliostat and then evaluating the heliostat area free from shading and blocking.

An analytical review of the former convolution codes can be found in [14], also including other Monte Carlo codes, such as SCT-HGM [25] (developed within the research project EU SIREC), and the more recent HFLD from the Chinese Academy of Sciences (CAS) [26,27] (published by 2010). More recent convolution codes not included in former reviews, such as CRS4-2 from the Italian CRS [28] and the MIT code [29], will be commented on later.

One conclusion of this former analytical review [14] is that the published codes leave several major questions unanswered concerning the details of the necessary layout optimization process for a

given set of input parameters (tower height, receiver dimensions, number of heliostats, etc.).

Therefore, issues such as where the layout optimization should commence, how and in which direction the optimization should proceed, what a practical management of the location updating of thousands of heliostats would be (in addition to them potentially shadowing and blocking neighbours), where the process should stop, etc., are not clear at all.

However, new proposals to respond to these major issues have already been put forward by the authors in the presentation of the *campo* code [14]. The key idea is based on the above explained f_{sb}-mirror density trade-off [15–17].

It has been suggested that with *campo*, the optimization would steadily progress from the densest layouts, with the worst shadowing and blocking factor (f_{sb}), but with good values for the other optical factors, see Eq. (1), towards expanded layouts, in which the f_{sb} is gradually improved, but the other factors gradually become worse. Thus, the maximum of the collected annual energy would be reached when the improvement in the f_{sb} was offset by the drop in the other factors in Eq. (1).

Logically, these proposals should be implemented in the *campo* code and checked against a real plant to assess their actual potential to help in the complex SPT optimization process.

In this study, *campo* will be checked against Gemasolar [7], the first solar power tower commercial plant with molten salt storage in the world. For the sake of convenience, the figure of merit of the optimizations performed here will be limited to the annual energy reaching the receiver, thus easing the assessment of new procedure abilities. Furthermore, it should be remembered that only a few key parameters, such as the number of heliostats (2650) [7], of the Gemasolar plant are really known, and many others are not available or not clear at all in the open literature, for example the receiver dimensions, the tower optical height (*THT* in Fig. 1), the detailed layout of the field, the typical meteorological year (TMY) used, etc. Logically, there is also no public information about capital costs.

In spite of the limited figure of merit used here, it should be taken into account that, strictly speaking, this layout optimization, maximizing the annual energy collected, should be repeated for each set of input parameters (defining the capital cost of the field), checked along a full optimization process seeking the lowest capital cost-annual energy ratio. Finally, it needs reiterating that this problem of how to distribute thousands of heliostats efficiently at any stage in full optimization remains an open question [15–29].

In conclusion, the main objective of this work is the validation, using the Gemasolar plant as a reference case, of the new procedure put forward here to find, step by step, the optimum layout of a large number of heliostats given a set of input parameters.

Therefore, the structure of this work is as follows. Section 2 provides a review of the development and current status of SPT and PT plants in Spain and USA showing, as commented on above, the huge boost that both technologies are experiencing, mainly in USA [9]. Section 3 reviews the full details of the models used by *campo* for the different factors that make up the optical efficiency, Eq. (1). These details were not supplied in [14] (with the exception of the shadowing and blocking factor). In addition, the most recent codes, i.e., CRS4-2 [28] and MIT [29], will be briefly analyzed here. Section 4 addresses the annual energy incident onto the receiver using the sunshine data measured in PSA (Almeria, Spain) for the GAST project [30]. Section 5 defines the optimization problem to be solved by *campo* based on the scarce open literature data on *Gemasolar* [7]. Section 6 puts the f_{sb}-other optical factors trade-off into practice, and also shows how the optimum search should progress and where it would stop. Section 7 compares the resulting optimized design layout yielded by *campo* with the scarce available data on Gemasolar. Finally, Section 8 concludes that the practical application of this classic trade-off supplies a clear, systematic and reproducible procedure (independent of the code used) to solve the complex problem of the optimized design of heliostat field layouts in SPT systems.

2. Short-term development and current status of CSP systems in Spain and USA

The UE DLR-ECOSTAR study [2], published in 2005, reviewed the potential deployment of seven CSP technologies including, among others, parabolic trough (PT) with thermal oil and SPT systems working with different heat transfer fluids (HTF), i.e., saturated steam, molten salt, and atmospheric and pressurized air. This study calculated for each technology the levelized electricity cost (LEC) for a reference system size of 50 MWe and analyzed the impact on cost of different innovations. This study [2] notices that since the absolute cost data for each of the reference systems are relatively close, choosing technologies for R&D prioritization (e.g., troughs vs. towers) does not seem feasible. This competition between technologies will be left to industrial entrepreneurship and market forces.

With this caveat in mind, one of the findings of the ECOSTAR study was that the lowest LEC (for 50 MWe) would be for two SPT systems, i.e., an SPT plant working with pressurized air followed by SPT systems working with molten salt. The solar power tower working with steam would be the fourth cheapest CSP technology.

Currently (November 2012), SPT systems with pressurized air have not reached the commercial scale yet, although it is still under active research, namely in DLR-Solar tower Jülich [31] with 1.5 MWe, and the PSA-SolHyCo project [32] with around 1 MWe.

On the other hand, SPT systems working with steam have reached the commercial scale with the cavity receiver plants PS10 (11 MWe) and PS20 (20 MWe) at full operation in Seville (Spain) [33], although their thermal storage capacity (steam) is low. Consequently, in periods without direct sunlight, the PS10 and PS20 electricity dispatches are limited to half an hour and 1 h, respectively [33].

Quite recently (November 2012), the same Spanish company [33] started the construction of a 50-MWe SPT plant (Khi project), with energy storage possible for 3 h, in South Africa [9].

The Gemasolar plant with a surrounding field and cylindrical receiver, also in Seville (Spain) [7], is currently the largest commercial-scale SPT plant (19.9 MWe) in operation in the world using molten salt storage, which allows for 15 h of electricity production without sunlight. However, it will be surpassed in the next 1–2 years by Crescent Dunes plant [8]. It has the same type of field and receiver as Gemasolar, but it is a much bigger SPT plant (110 MWe, i.e., full commercial scale), also using molten salt with 8–20 h of thermal storage, currently under construction in Nevada desert (USA).

The main thermodynamic advantage of SPT systems with molten salts storage (MSS) over parabolic trough working with thermal oil (but also with MSS) is the receiver outlet temperature of the HTF used, although it also involves much more expensive SPT central receivers. In SPT systems, the usual outlet temperature of the molten salts is 565 °C [8,34] with an inlet temperature in Crescent Dunes of 288 °C [8] and 290 °C in Gemasolar [34]. This means an increase in the molten salt temperature (ΔT) in the receiver of 277 °C (Crescent Dunes) or 275 °C (Gemasolar), thus reducing the amount of salt by a third with respect to parabolic trough plants with thermal oil as primary HTF, in which ΔT=(94 °C=386–292) is limited by the oil hot set point (393 °C) [34]. Therefore, the size of the thermal storage tanks

would also be reduced by a third. In addition, this higher receiver outlet temperature allows for a more efficient, higher pressure reheat turbine, thus drastically improving the efficiency of the thermodynamic cycle in SPT systems with MSS [35] in relation to parabolic trough plants.

In spite of these economic and thermodynamic advantages of SPT plants on PT systems, parabolic trough technology is currently far more widespread in Spain and USA than SPT systems, probably due to technological (the complexity of SPT plants is higher than PT ones) and economic reasons. So in Spain, the operational PT systems are already at 50 MWe, whereas the sizes of the working SPT systems are still in a pre-commercial scale (10–20 MWe). The Projects & Markets Tracker application of CSP Today [9] shows a total (including operational, under construction or planned) of 63 CSP technologies projects in Spain, of which 50 projects are parabolic trough, almost all 50 MWe. In contrast, there are only three SPT plants in operation, namely the aforementioned PS10 (11 MWe), PS20 (20 MWe) and Gemasolar (19.9 MWe), none under construction and only one more planned, Termosolar Alcazar (50 MWe).

The situation is rather different in USA, in which out of a total of 45 CSP systems (operational, under construction or planned) 17 are SPT systems and 24 are parabolic trough plants [9]. Out of the 14 operational PT plants, three are in the 1–5 MWe range and the remaining 11 plants range from 14 to 89 MWe. In contrast, there are only two operational SPT plants, SierraSunTower (5 MWe) and Coalinga (about 13 MWe, although this plant is indeed the world's largest solar thermal enhanced oil recovery demonstration facility).

However, there are five SPT plants currently under construction. They range from 110 MWe (the aforementioned Crescent Dunes project [8]) to 280 MWe (Mojave Solar Project). Furthermore, the nine planned SPT projects in USA range from 150 MWe to 750 MWe. These sizes are in agreement with a quite recent reported forecast of the cost for SPT with MSS [8]: the cost curve would seem to have a broad minimum between 500 and 750 MWe (beyond this limit, larger stations will be composed of modules of these large sizes).

The near future is similar for parabolic trough, so out of the eight plants under construction or planned, five have a size $\geq$ 200 MWe, with a maximum of 340 MWe (Hualapai Valley Solar Project).

To conclude this brief review of the current status of CSP technologies in Spain and USA, it would seem that, after some years of research and tests, the economic and thermodynamic arguments, in addition to clean energy incentive programs, have encouraged the construction of SPT systems at full commercial scale in USA. On the other hand, several years' experience with a reliable operation of PT power plants in the range of 50 MWe and above would also have brought about a drastic increase in its scale, i.e., about six times bigger.

Therefore, the far more mature CSP technologies are currently parabolic trough and solar power tower, for which sizes in the 300 MWe range are expected to be operational in the next 3–4 years in USA. Now the battlefield between market forces has been moved from Spain to USA. Obviously the next step for Spain should be to increase the size of the next CSP plants drastically, although the response would seem to be on its way with the Khi project (South Africa).

3. Models of the instantaneous optical efficiency factors used in *campo*

Following Eq. (1), the models used by *campo* for the different optical efficiency factors are described. At the same time, the more recent CRS4-2 [28] and MIT [29] codes will be briefly reviewed for the most critical components, i.e., the shading and blocking factor and interception or spillage efficiency terms. Notice that interception is not addressed in [28].

3.1. General coordinate system, incidence cosine and Sun position

The basic coordinate system and the incidence cosine calculation are, in general, common for all the codes [14–29]. However, the model of the sun position may differ among the codes.

Campo follows the general coordinate system defined in DELSOL3 [18]. East is in the positive X direction and North is in the positive Y direction, whereas the Z axis coincides with the tower axis and is directed at the zenith. The origin of coordinates is placed in the Z axis at the same height as the centres of the heliostats in a plane field. Polar (zenith) angles are measured from vertical. Azimuth angles are measured clockwise from the South. Also following DELSOL3 [18], there are three basic unitary vectors with the heliostat centre as the origin: the sun vector **s**, pointing to sun; the normal vector **n**, directed along the normal heliostat; and **t**, the reflected vector directed at the aim point on the receiver. See Fig. 1.

The incidence cosine is merely the dot product of unitary vectors **n** and **s**, or **n** and **t**,

$$\cos\omega(x,y,t)=\mathbf{n}(x,y,t)\cdot\mathbf{s}(\text{location},t)=\mathbf{n}(x,y,t)\cdot\mathbf{t}(x,y) \tag{3}$$

where (x, y) are the general coordinates of the analyzed heliostat surface centre, t is the solar time and location stands for the plant's geographical location (latitude and longitude). Gemasolar's latitude is 37.46°N (Seville), very similar to that of PSA (Almeria), i.e., 37.1°N.

Finally, the model of the sun position in *campo* is the same as in DELSOL3 [18].

3.2. Sener heliostats, reflectivity and cleanliness

Gemasolar [7] is the plant established as a reference in this work. The total dimensions of Sener heliostats used in Gemasolar have been derived by the authors from the scarce data reported in [36], namely total height LH = 9.752 (m) and total width LW = 12.305 (m). Thus the total area of the heliostat is $A_h = \text{LH}\times\text{LW} = 120$ (m^2) and its total diagonal DM = 15.7 (m). The effective mirror area A_m (excluding the gaps between the individual facets of the heliostat) has been reported as $A_m = 115.7$ (m^2) [37].

The nominal reflectivity of the Sener heliostats used in the Gemasolar plant is not reported in the open literature reviewed [7,34–38]. As a reasonable alternative, a nominal reflectivity of 0.88, which is suggested in [27] concerning the heliostats used in PS10 [32], which has similar dimensions to the Sener heliostat, is used here (and also used by MIT code [29]). The actual reflectivity would therefore be

$$\rho = 0.88(\times 0.95) \tag{4}$$

where the factor of 0.95 multiplying by the nominal value would be the nominal cleanliness [1] of the mirrors, which would depend on the plant's maintenance level.

3.3. Atmospheric attenuation factor

Atmospheric attenuation can be calculated simply as a function of the distance between the heliostat and receiver D (m), see Fig. 1, following MIRVAL [22]

$$f_{\text{att}} = 0.99321 - 0.000176D + 1.97\times 10E{-}8D^2 \quad (D \leq 1000\ \text{m}) \tag{5}$$

This formula was extended in [19] for the range above 1 km to give realistic results for larger slant ranges,

$$f_{\text{att}} = e^{-.0001106D} \quad (D > 1000 \text{ m}) \tag{6}$$

The MIT code also uses the same model.

3.4. Intercept factor

In a recent comparison [39] between the HFLCAL [19–20] and UNIZAR [40] models of the energy image sent by a single heliostat, which tests both models against actual spots measured for first generation heliostats, it is concluded that the HFLCAL model is much simpler and slightly more accurate than the UNIZAR model.

The HFLCAL [19–20] assumes all heliostats have well-canted concentrating facets of spherical curvature. The flux density expression of the HFLCAL [19] is merely a circular normal distribution, so the intercepted fraction of power is [19]

$$f_{\text{int}} = \frac{1}{2\pi\sigma_{\text{tot}}^2}\int_{(x')}\int_{(y')} \exp\left(-\frac{x'^2+y'^2}{2\sigma_{\text{tot}}^2}\right) dy' \cdot dx' \tag{7}$$

where σ_{tot} is the total standard deviation result measured on the image plane [40], i.e., a plane normal to the unit vector **t**, and with coordinates (x', y').

The total deviation σ_{tot} in HFLCAL is the result of the convolution of the four Gaussian error functions considered [19], namely sunshape error, with standard deviation σ_{sun}, beam quality (σ_{bq}) associated with mirror slope errors, the astigmatic effect (σ_{ast}), and, finally, the tracking error (σ_t). Then σ_{tot} is

$$\sigma_{\text{tot}} = \sqrt{D^2\left(\sigma_{\text{sun}}^2 + \sigma_{\text{bq}}^2 + \sigma_{\text{ast}}^2 + \sigma_t^2\right)} \tag{8}$$

where D is the slant range, i.e., the distance between the heliostat centre and the aim point in the receiver (also used in the former attenuation factor).

For σ_{sun}, the standard deviation of the Gaussian equivalent to the sunshape measured in PSA [40], i.e., 2.51 mrad, will be used here.

The standard deviation of beam quality σ_{bq} is related to the slope error σ_s (deviations in the mirror curvature from the ideal shape and waviness and roughness of the reflecting surface), which is defined with respect to the surface normal error [19]. Its effect is, therefore, doubled in the reflected ray

$$\sigma_{\text{bq}}^2 = (2\sigma_s)^2 \tag{9}$$

After some optical quality tests of Sener heliostats, an elliptical Gaussian distribution (here assumed that of the slope error) with σ_h=1.02 mrad (horizontal axis) and σ_v=0.85 mrad (vertical axis) has been reported [37]. Following [41], the equivalent circular Gaussian error distribution would be

$$\sigma_s \approx \sqrt{\frac{1.02^2 + 0.85^2}{2}} = 0.94 \text{ mrad} \tag{10}$$

Also in [37] after 240 tracking tests of Sener heliostats under low wind speed conditions, an average standard deviation of the Gaussian tracking error of σ_t=0.63 mrad has been reported.

Finally, following [19], the standard deviation of the astigmatic effect is

$$\sigma_{\text{ast}} = \frac{\sqrt{0.5\left(H_t^2 + W_s^2\right)}}{4D} \tag{11}$$

where H_t and W_s are the image dimensions in the tangential and sagital planes at a distance D from the mirror, respectively. Their values are [19]

$$H_t = d\left|\frac{D}{f} - \cos\,\omega\right|; \quad W_s = d\left|\frac{D}{f}\cos\,\omega - 1\right| \tag{12}$$

where f is the focal distance, which is equal to D when the heliostat is focused on its slant range as usual, and d is a general dimension of the heliostat. This work has assumed that d is equal to the square root of the whole heliostat area

$$d = \sqrt{\text{LW} \times \text{LH}} \tag{13}$$

Concerning the integration limits in Eq. (7), the intercept factor will be the integral on the contours of the cylindrical receiver for a surrounding field as in Gemasolar [37]. But here the integration is made on the image plane, normal to the unitary vector **t**. So the cylindrical receiver is seen by the heliostat as a rectangle with a width equal to the diameter of the receiver 2 × RR (radius RR), and a height HR × cosγ. HR is the actual height of the receiver and γ is the complementary angle of β, β being the angle between **t** and the vertical, see Fig. 1. If **t** coincided with axis z, β would be zero and cosγ=0.

On the other hand, MIT code defines a regular orthogonal mesh on the heliostat surface [29]. For the centre of each rectangular cell, the direction of the reflected ray is determined as a function of the direction of the sun and the surface normal direction of the cell. Then the error cone (including astigmatism, surface and slope errors, and sunshape) of the reflected ray is approximated with flux density proportional to an angular Gaussian distribution. Finally, this reflected ray is intersected with the receiver plane and integration over the receiver edges is performed with the help of the inverse error function.

In the MIT code, the shadowing and blocking factor and the interception factor are validated using the ray-tracing tool SolTRACE [23–24]. The number of cells on each heliostat surface used for the validation ranges from 9 to 100. Then the calculation of the interception factor for each and every heliostat in the field would mean (a maximum of) 100 integrations.

Apart from the fact that this figure may be rather high in a full optimization process with thousands of heliostats, this discretization poses the problem that treating the reflected rays locally on the heliostat surface would involve assigning the standard deviations of the different Gaussian errors locally as well, which is obviously not at all easy. Global (for the entire heliostat surface) standard deviations are then used in the comparisons of the MIT code.

Finally, the accuracy of the interception factor would indeed depend on the ability to reproduce actual energy spots sent by a heliostat. It would, therefore, be necessary to compare and fit [39,40] measured energy images of the heliostats with a flux density model.

3.5. Basic layout, location of blocking and shadowing heliostats and f_{sb} calculation

As these issues have already been addressed in depth by the authors in a recent work [14], only a brief review will be given here. The basic layout in *campo* is a radial stagger configuration, which has proved to be extremely efficient in codes like RCELL [15–17] and DELSOL3 [18]. Furthermore, this layout limits the potentially blocking heliostats to only three, whose relative locations with respect to the blocked heliostat are immediate [14].

The radial staggered distribution creates "prearranged" grids, i.e., the angular azimuth spacing (degrees) should be kept constant between contiguous heliostats in the same row throughout each zone in which the field is divided. In contrast, the length of the azimuth spacing (metres) between adjacent heliostats will grow gradually with the radius of the row. Any zone in the field

would then be complete when we could place an extra heliostat between two adjoining heliostats in the same row. Consequently, angular azimuth spacing is regularly decreased in passing to an outer zone.

As the azimuth angular spacing is kept constant throughout each zone, the problem of how to locate the shadowing heliostats relative to the moving position of the analysed heliostat while the field is expanded can be addressed with some ease.

The field is divided into sectors in which the relative position of the potentially shadowing heliostats is kept along the optimization process. The selection tests of the shadowing heliostats for each sector (a maximum number of three heliostats for each sector and basic function of the azimuth) are made for the densest layouts, thus ensuring the worst case scenarios are covered.

Notice that the former three blocking heliostats are also projected following the sun vector. Therefore, a total of six heliostats are checked for shadowing and three for blocking, i.e., a total of nine projections on the surface of the analysed heliostat. The individual calculation [14] of the shadowing and blocking factor f_{sb} in Eq. (1) projects the centres of neighbouring heliostats following the sun or the tower [42,43] and then uses the Sassi procedure [44], which efficiently manages the overlapping of the projected outlines to find the fraction of the heliostat's whole area free from shadings and blockings f_{sb}.

As already mentioned in the introduction, *campo* would start the optimization process from the densest field then proceed towards expanded fields increasing the radial distance between consecutive rows, but without changing the azimuth angular spacing in each zone. Therefore, the actual location of blocking and shadowing heliostats will certainly change with the radial expansions, but their relative location (through relative indexation) will not. Thus, the necessary actual location update of the potentially shadowing and blocking heliostats for each heliostat in the field after any change in the layout (only radial ones) is greatly eased.

Finally, again highlighting the other factors-f_{sb} factor trade-off, see Eq. (1). From Eqs. (5)–(8), it seems clear that the further the heliostat (from the receiver), the lower the intercept and the higher the atmospheric attenuation, i.e., the lower the attenuation factor. Thus, the densest fields will have the highest attenuation and intercept factors. Quite the opposite, the closer to each other the heliostat rows are, the higher the shadings and blockings, i.e., the densest fields will have the lowest f_{sb} factor. This trade-off is the prime mover of the optimization process.

CRS4-2 code [28], as MIT code does, also splits the surface of the heliostat into cells and the centres are projected in the directions of the sun and receiver for shading and blocking, respectively. Again the problem would be the computational load of projecting several points each time the shadowing and blocking factor have to be worked out. *Campo* only projects the centre of the shadowing and blocking heliostats onto the heliostat analyzed [14] because it is assumed that the heliostats are in parallel planes (this would be the worst case).

4. Annual energy reaching the receiver and the TMY used

As mentioned in Section 1, the annual energy reaching the receiver is the sum of the instantaneous energy produced by the whole field of heliostats along the instants of time sampled in a typical meteorological year (TMY). The TMY is a key piece of information in the optimization process and should be based on direct normal solar intensity measurements over several years.

Unfortunately, there is no public information on the TMY used in the Gemasolar plant (Seville 37.46° N). As an alternative, data for PSA (Almeria 37.1° N) used in the GAST project [30] is used, see Tables 2 and 3 in [45]. There are only seven months considered because there is symmetry of the sun position and its direct intensity with respect to summer solstice (June), see Table 2 in [45]. December is not in this symmetry and is, therefore, also included.

Each month j has a total of nh_j hours of sunshine (plus the hours of its symmetric month in the year), see Table 3 in [45]. Whereas the I_D (kW/m^2) is given every hour from sunrise (a minimum of 15° of sun elevation over horizon) to noon (again by symmetry) for only one day (in this work, it is usually taken on the 21st) on behalf of the whole month. Thus, the annual energy E_R reaching the receiver along the TMY would be

$$E_R \approx A_m \sum_{\text{field}} \left[\sum_{j-\text{month}} \overline{P}_{m,j} \times nh_j \right] \tag{14}$$

where A_m (m^2) is the net mirror area of the heliostat and $\overline{P}_{m,j}$ is the average of the former instantaneous power sent by a single heliostat, see Eq. (2), for the representative day of month j

$$\overline{P}_{m,j} = (1/nd_j) \sum_i (\eta_i \times I_{D,i}) \tag{15}$$

where in turn nd_j is the number of hours considered (from sunrise to sunset) in the representative day of the month j. Now it is convenient to translate this single average power $\overline{P}_{m,j}$ to an individual optical performance average of month j $\overline{\eta}_j$, previously calculating an average direct normal intensity for the representative day of the month $\overline{I}_{D,j}$

$$\overline{\eta}_j = \frac{(1/nd_j)\sum_i (\eta_i \cdot I_{D,i})}{(1/nd_j)\sum_i I_{D,i}} = \frac{\overline{P}_{m,j}}{\overline{I}_{D,j}} \tag{16}$$

Now substituting the expression of $\overline{P}_{m,j}$, derived from Eq. (16), into Eq. (14) we have

$$E_R \approx A_m \sum_{\text{field}} \left[\sum_{j-\text{month}} \overline{\eta}_j \times \overline{I}_{D,j} \times nh_j \right] \tag{17}$$

Then the annual average of the individual optical performance η_{annual} of any heliostat can be found as

$$\eta_{\text{annual}} = \frac{\sum_{j\text{-month}} \overline{\eta}_j \times \overline{I}_{D,j} \times nh_j}{\sum_{j\text{-month}} \overline{I}_{D,j} \times nh_j} \tag{18}$$

The denominator of Eq. (18) is usually called the annual direct normal intensity or *DNI* in kW h/m^2/year

$$DNI = \sum_{j\text{-month}} \overline{I}_{D,j} \times nh_j \tag{19}$$

For the GAST project (Almeria) [30], the *DNI* is 2267.9 (kW h/m^2/year) whereas for the Gemasolar project [46] $DNI = 2062$ (kW h/m^2/year).

Deriving the expression of the numerator of Eq. (18) (including the *DNI* definition) and substituting it in Eq. (17), we find that

$$E_R \approx A_m DNI \sum_{\text{field}} \eta_{\text{annual}} \tag{20}$$

Working out a whole field average η_{field} of the single annual optical efficiencies, obviously based on the total number of heliostats in the field N_{hel},

$$\eta_{\text{field}} = (1/N_{\text{hel}}) \sum_{\text{field}} \eta_{\text{annual}} \tag{21}$$

we can finally arrive at the annual energy reaching the receiver on the basis of η_{field} as

$$E_R \approx A_m DNI\, N_{\text{hel}}\, \eta_{\text{field}} \tag{22}$$

In conclusion, to obtain the annual energy produced, we should first calculate the individual instantaneous efficiency of each heliostat in the field (2650 heliostats in the Gemasolar plant [7]) at every instant of time considered, i.e., 35 times for the GAST project (see Tables 2 and 3 in [45]). They should then be appropriately combined considering the abovementioned symmetries to finally find the annual energy.

5. Reference case based on Gemasolar for *campo* optimization

Table 1 shows the information collated in several sources [7,34–38] regarding the details of the Gemasolar collector field. Some of them have already been commented on in Section 3 and others, concerning the layout, will be explained later in Section 7. Only the selection of the receiver dimensions and tower optical height will be referenced here.

In [35], it is stated that a range of dimensions were analyzed for the Gemasolar receiver, namely diameter (8 to 10 m) and height (9 to 11). Here, we assume an economic receiver with a radius of RR=4 m and a height of HR=2RR+1.

In [37], it is reported that the receiver is placed at the top of a 140-m tower. However, see Fig. 1, it is the optical tower height that is really needed. For example, in [8], given nominal conditions for some SPT plants, it is stated that the tower height includes the receiver. Assuming the same for Gemasolar, we subtract 5 m from half the receiver height plus about 5 m of the heliostat pedestal from the previous 140 m to end up with a tower optical height (THT) of around 130 m.

In conclusion, the optimization problem to be solved is to find the optimum layout of 2650 Sener heliostats [36] yielding the highest annual efficiency (annual energy) for a collector field defined by the reference case in Table 1, which will be placed in Almería due to the TMY used.

Campo starts off with a larger field of heliostats, as HFLCAL does [20], so every optimization process manages 3864 heliostats=8 rows × 46 (368)+16 rows × 92 (1472)+11 rows × 184 (2024) for each of which the annual average of the optical efficiency is calculated. Finally, the boundary of the field is the result of applying the condition that only the first 2650 heliostats with the best efficiency (out of a total of 3864 heliostats) will be finally selected.

6. Results of the new *campo* procedure for the optimal layout of heliostat fields

With reference to the graphic representation of a heliostat field from a top view, the footprint of any heliostat would be a circle of diameter DM, i.e., the diagonal of the total area (15.70 m for Sener heliostats, see Table 1), plus any additional separation distance, in this case $d_{sep}=0$ has been used in *campo*.

As we have already noted, *campo* would commence the optimization search from the densest possible layout, with the worst shadowing and blocking factor f_{sb} but with good values for the other optical factors in Eq. (1), progressing towards gradually expanded distributions.

Fig. 2a shows the map of the annual averaged optical efficiency η_{annual}, Eq. (7) for the densest possible field, which corresponds to a radial separation between two consecutive rows of $\Delta R=\cos30^\circ \times$ DM, i.e., 0.866DM, constant throughout the field. The field average of this annual averaged optical efficiency (η_{annual}), in short field efficiency η_{field}, and the number of heliostats for the three zones considered (a total of 2650 heliostats as in Gemasolar), in addition to the zone averaged efficiencies, are also reported. Remember that every optimization process starts with 3864 heliostats, thus the specific trimming of the field is merely the result of selecting the first 2650 heliostats with the best performance.

The field average for the densest layout η_{field} is 51.335%. This would be the lowest field efficiency we would obtain because, as we gradually expand the field only increasing radial distances, we should see that η_{field} increases, since f_{sb} would improve due to a higher separation between consecutive rows, although the other optical factors in Eq. (1) worsen.

This key hypothesis of the work is confirmed by Fig. 2b (and the following ones), in which the radial separation is increased to one heliostat diameter, namely $\Delta R_1=\Delta R_2=\Delta R_3=1$DM for zones 1, 2 and 3, respectively; resulting in a higher field efficiency of 53.519%, i.e., more than two points higher.

We could wonder what would happen if we kept the radial increment of $\Delta R_2=\Delta R_3=$DM, but ΔR_1 was equal to 0.866DM. Remember that zone 1 is the closest to the tower where blocking is the lowest, so this efficiency should not be very affected, but zones 2 and 3, with far more heliostats than zone 1, would be moved into better efficiency places closer to the tower. An efficiency increment of about 0.14% is now obtained

Table 1
Gemasolar data and reference case used by *campo*.

Parameter	Gemasolar value	Reference case in *campo*
Tower optical height (THT)	140 m [37]	130 m (assumed)
Receiver radius (RR)	4–5 m [35]	4.0 m (assumed)
Receiver height (RH)	9–11 m [35]	9.0 m (assumed)
Heliostat total height (LH)	9.752 m, derived from [36]	9.752 m
Heliostat total width (LW)	12.305 m, derived from [36]	12.305 m
Heliostat total diagonal (DM)	15.7 m, derived from [36]	15.7 m
Heliostat total area (AH)	120 m^2, derived from [36]	120 m^2
Heliostat mirror area (AM)	115.7 m^2 [37]	115.7 m^2
Standard deviation surface error (σ_s)	0.94 mrad [37,41]	0.94 mrad
Standard deviation tracking error (σ_t)	0.63 mrad [37]	0.63 mrad
Standard deviation of sunshape (σ_{sun})	Proprietary data	2.51 mrad [45]
Effective reflectivity (ρ)	Proprietary data	0.88 × 0.95 [1,27]
Number of zones in the field	3–4	3
Heliostat field layout of 1st zone	Aligned and radial staggered ΔR=(1–1.2)DM	Staggered (ΔR=DMcos30°)
Number of heliostats in first row	31 (0.57 × THT) [34,37]	46 (0.82 × THT) (assumed)
Heliostat field layout of 2nd & 3rd zones	Staggered, ΔR variable	Staggered, ΔR constant
Number of heliostats in 2nd zone first row	72 [37]	92
Extra separation distance (d_{sep}) zones 2–3	(0.4–0.58)DM [37]	0 m
Number of heliostats in the field	2650 [7]	2650
Latitude location	37.46°N (Seville)	37.1°N (PSA)
Typical meteorological year (TMY)	Proprietary data	PSA [30]
Annual normal direct intensity	2062 kW h/m^2/year [46]	2268 kW h/m^2/year [30]

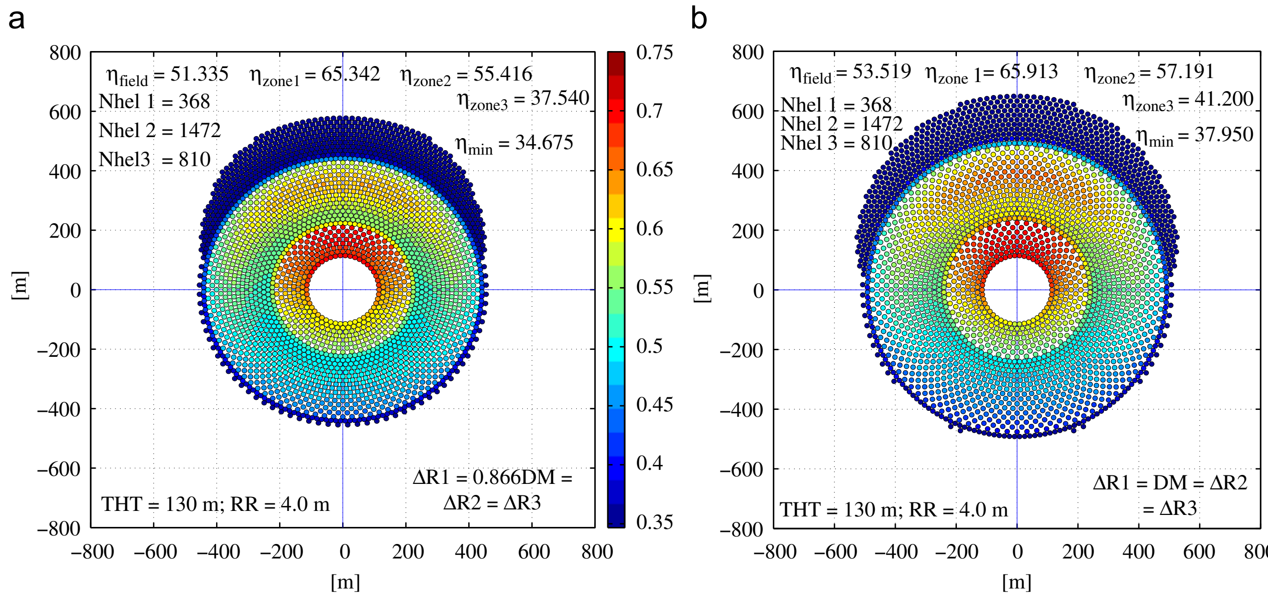


Fig. 2. (a) Map of the annual efficiency for $\Delta R_1=\Delta R_2=\Delta R_3=0.866$DM. (b) Map of the annual efficiency for $\Delta R_1=\Delta R_2=\Delta R_3=1$DM.

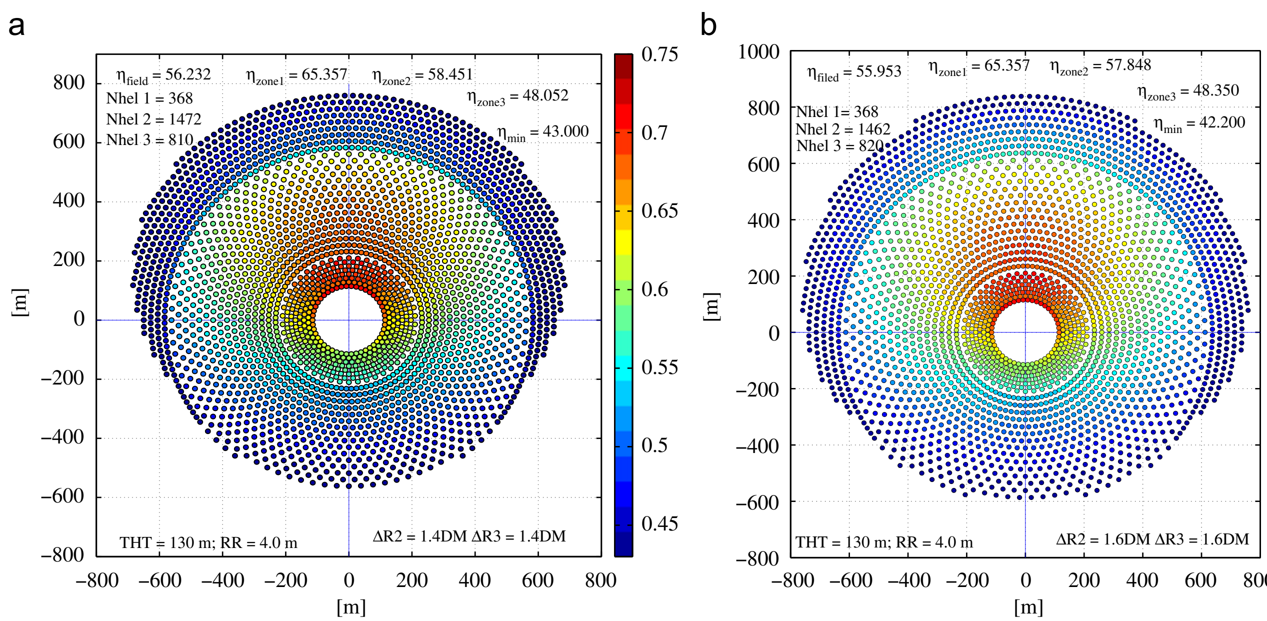


Fig. 3. (a) Map of the annual efficiency for $\Delta R_1=0.866$DM, $\Delta R_2=1.4$DM and $\Delta R_3=1.4$DM. (b) Map of the annual efficiency for $\Delta R_1=0.866$DM, $\Delta R_2=1.6$DM and $\Delta R_3=1.6$DM.

($\eta_{\text{field}}=53.662\%$), see Fig. A1, in electronic Appendix A. From now until the end of the optimization process, the radial separation in zone 1 will be held at a constant value of $\Delta R_1=0.866$DM.

Then the field expansion proceeds to augment the radial separations in zones 2 and 3 to $\Delta R_2=\Delta R_3=1.2$DM, constant in the zones. The field efficiency keeps on growing (55.58%) see Fig. A2 in electronic Appendix A.

Again ΔR_2 andΔR_3 are increased and now set to 1.4DM, see Fig. 3a, and a higher efficiency ($\eta_{\text{field}}=56.232\%$) is attained again, but in passing to $\Delta R_2=\Delta R_3=1.6$DM, the field efficiency falls a little until 55.953%, Fig. 3b. The reason is the worsening of zone 2, where local efficiency falls slightly from $\eta_{\text{zone 2}}=58.451\%$ in Fig. 3a to 57.848 in Fig. 3b. On the contrary, the efficiency in zone 3 improves in passing from 1.4DM to 1.6DM (zone 3 is the most affected by blocking), but its rather slight increment cannot counteract the field efficiency drop of zone 2. It could be said that $\Delta R_2=1.4$DM could be seen as a local maximum for zone 2, i.e., if ΔR_2 were further increased, the f_{sb} improvement in zone 2 would be surpassed by the worsening of the other optic factors in Eq. (1).

Therefore, from now on ΔR_2 will be kept equal to 1.4DM. Fig. 4a confirms the convenience of this setting, so a new increase in field efficiency is obtained with $\Delta R_2=1.4$DM and$\Delta R_3=1.6$DM. Now η_{field} almost reaches 57% (56.953%), whereas Fig. 4b presents a new increment (although rather slight) in efficiency when zone 3 is again expanded to $\Delta R_3=1.8$DM, which now surpasses 57% attaining a performance of 57.215%.

Finally Fig. 5a shows the optimum heliostat field with the maximum field efficiency reached (57.232%), which from Eq. (11) also means maximum annual energy collected in the receiver, obtained with $\Delta R_1=0.866$DM, $\Delta R_2=1.4$DM and$\Delta R_3=2.0$DM. This is a very flat maximum because increasingΔR_3 to 2.2DM in Fig. 5b only produces a slightly lower η_{field} (57.158%) than the former optimum,

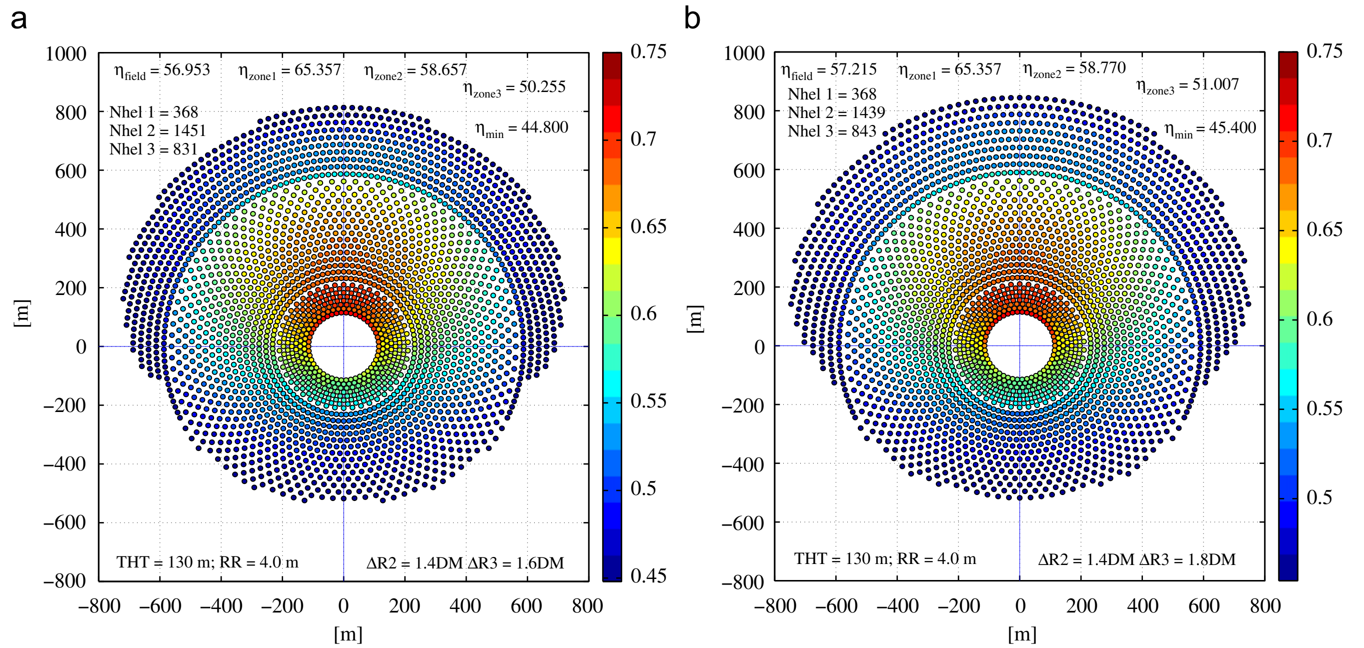


Fig. 4. (a) Map of the annual efficiency for ΔR_1=0.866DM, ΔR_2=1.4DM and ΔR_3=1.6DM. (b) Map of the annual efficiency for ΔR_1=0.866DM, ΔR_2=1.4DM and ΔR_3=1.8DM.

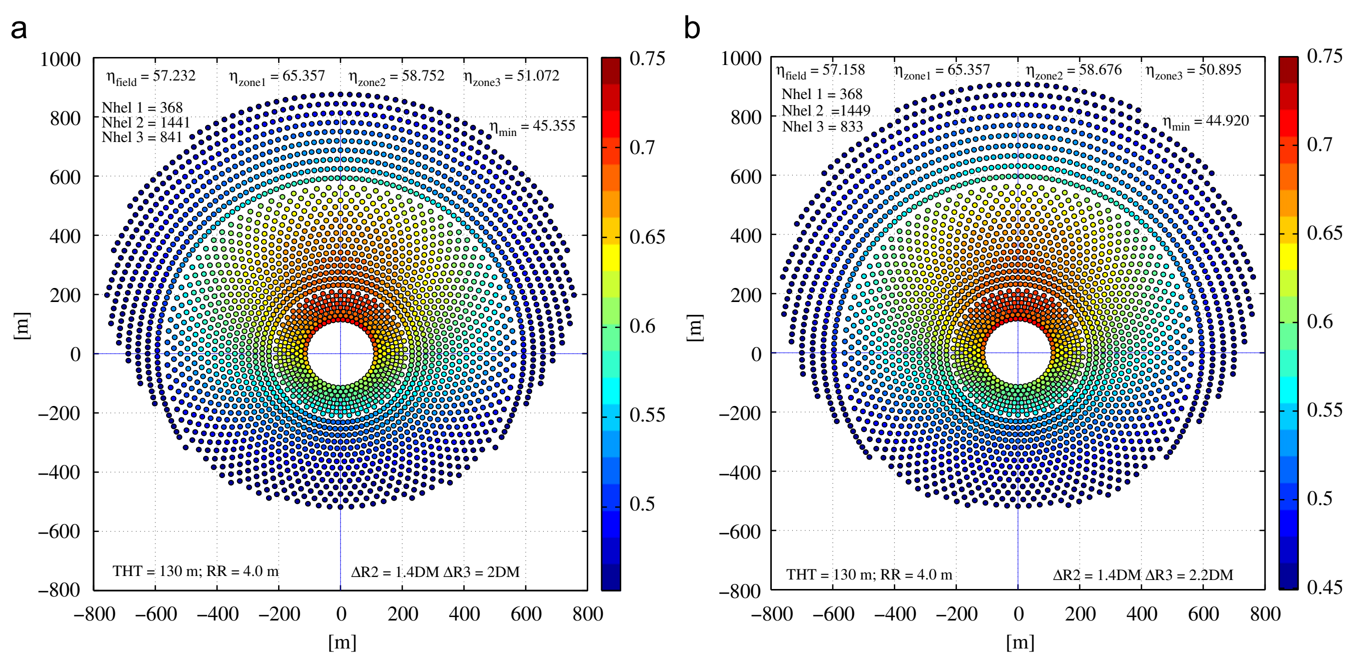


Fig. 5. (a) Map of the annual efficiency for ΔR_1=0.866DM, ΔR_2=1.4DM and ΔR_3=2.0DM. (b) Map of the annual efficiency for ΔR_1=0.866DM, ΔR_2=1.4DM and ΔR_3=2.2DM.

Fig. 5a. Thus with ΔR_3=2.2DM, the f_{sb} factor improvement due to the gradual expansion of the field starts to be offset by the fall in the remaining optical efficiency factors, Eq. (1).

Fig. A3 of Appendix A verifies that a field efficiency optimum is actually found. Therefore, following the field expansion using ΔR_3=2.4DM, η_{field} is now lower than before, namely 57.064%, thus confirming the downtrend.

In Fig. 6 the new procedure for layout optimization is summed up. It would seem that each zone of the field had their own local maximum, which can be easily detected along the expansion process by an efficiency drop.

The former process has held the radial increment constant within each zone. Now we briefly explore the possible advantages of linearly varying the radial increment for zones 2 and 3. Fig. A4 shows the annual averaged efficiency map for a layout with ΔR_2 and ΔR_3 with linear variations with R in such a way that the radial increment at the end of the zone matches the former maximum found using constant increments. The improvement found is extremely low, i.e., now 57.238% and formerly 57.232%. Finally, Fig. A5 checks to enlarge these linear variations of ΔR. The result is a clear worsening due to an excessive separation from the tower.

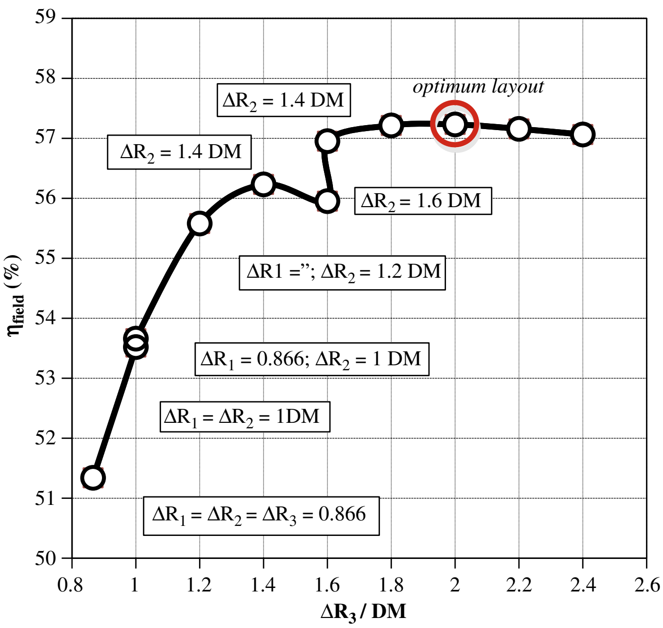


Fig. 6. Field efficiency vs. radial expansion of the layout.

7. Comparison of the *campo* optimum layouts with Gemasolar plant data

To compare the above optimum layouts found with *campo*, we use a diagram of the Gemasolar layout found in [37]. It presents a serious problem, given that in the printed drawing the North–South axis length is deformed (reduced) with respect to the East–West axis, so this length difference had to be fixed. Therefore, the following information about Gemasolar and Table 1 should be taken with extreme care.

7.1. General dimensions of the heliostat field

Concerning Gemasolar, it would seem that its layout would stretch, following the North axis, until about 870 m (from the tower), whereas towards the South it would extend until around 550 m. Furthermore, to the East and West axis, the field symmetric side could measure about 735 m.

With *campo*, the resulting optimum layout, see Fig. 5a, reaches 875 m along the North axis and 520 m towards the South axis, and it has a lateral side of 760 m. Another layout produced by *campo*, see Fig. 5b, with an efficiency very close to the optimum, although slightly lower (57.158%), arrives at 905 m along the North axis and 520 m towards the South, with the lateral side now 760 m.

On the other hand, the characteristic trimming of the outer rows (zone 3) of the field shown in Figs. 5a–b is merely the result of applying the condition of only adding, in the final layout, the best 2650 heliostats to the initial set of 3864 heliostats calculated.

In the Gemasolar layout diagram [37], this trimming is very similar to the *campo* results of Figs. 5a–b although the Gemasolar inner row of zone 3 almost reaches 550 m towards the South axis, whereas in Figs. 5a–b it is only 350 m and 375 m, respectively.

Indeed, Fig. 5b is quite similar to the Gemasolar layout in the outer rows, so the last row in the upper part (North) of the field has around 28 heliostats in Gemasolar whereas *campo* gives 27 heliostats. The trimming of the second outer row supplies about 41 heliostats in Gemasolar but *campo* obtains 48 heliostats. This growing difference in the trimming of the outer rows between *campo* and Gemasolar would justify the former different trimming length of the inner rows of zone 3.

7.2. Arrangement of the heliostats by zones

It would seem that Gemasolar has a very dense first zone where some rows are aligned, which has a clear advantage over the radial staggered layout, i.e., the number of heliostats in a row grows from one row to the next outer row. The potential drawback for aligned arrangements would be the increment in shadings and blockings.

This Gemasolar aligned arrangement of zone 1 (indeed it would seem that there are two zones, i.e., the first one with five aligned rows and the second with five rows as well, but radial staggered) allows ten rows with a total of approximately 610 heliostats, which can be compared with the 368 heliostats for zone 1 in *campo,* with eight rows (due to the full radial staggered configuration).

The radial increment between the rows in Gemasolar zone 1 varies with *R* and it would be about 1DM in the first subzone, but would reach around an average of 1.2DM in the last five rows of this global zone 1 [37]. On the other hand, the footprint would seem to be 1DM ($d_{sep} \approx 0.0$) in zone 1.

Zone 2 of Gemasolar is radial staggered with about 72 heliostats per row (92 heliostats in zone 2 of *campo*) and seventeen rows. The radial increment also varies with *R*, with an average value for the 17 rows of about 1.15DM. However, the footprint of each heliostat is about 1.45DM, which is rather different from the assumptions made with *campo* (1DM).

Finally, zone 3 is also radial staggered with around $2 \times 72 = 144$ heliostats per row (194 heliostats in *campo*). The footprint is around 1.6DM, but the radial increment (variable) ranges from 1.5DM in the first rows to 2.4DM in the last couple of rows (1.91DM in average).

In conclusion, in Gemasolar the azimuth separation between adjacent heliostats in zones 2 and 3 (a heliostat footprint of 1.45–1.6DM) has been enlarged taking precedence over radial distances. The probable objective would be to reduce radial distances without worsening shading and blocking then decreasing the longer distances (*D*) between heliostats and receiver. This would have three pros, namely the lower the distance the higher the intercept, and then the lower the receiver dimensions needed the lower its expensive capital cost, and, finally, the lower the receiver the lower its thermal losses. In *campo*, priority has been given to radial separation whereas the azimuth distance has been held at minimum values.

However, in the end, both layouts have quite similar values for the longest distances between heliostats and receiver ($Y = 870$ m) in spite of having rather different heliostat arrangements in the field. The reason is that the azimuth length controls the number of heliostats that can be put in a row of a given radius. Therefore, for a constant number of heliostats in the field, Gemasolar has to place more rows to fulfil this former condition. In the end, the longest distance is similar for both options.

7.3. Annual efficiency of the field

The value of the optimum field efficiency in Gemasolar is obviously proprietary information and it has not been possible to establish any comparison. However, former estimates of the annual collector efficiency forecasted by Sargent and Lundy [1] give a value of 56%. In this same study, Sun-Lab predicts for the mid-term (2008) and the long-term (2020) a collector annual efficiency of 56.3% and 57%, respectively. This would mean that *campo* would have given about a 1.24% higher efficiency than that

predicted by Sargent and Lundy, but less than 1% of difference with the Sun-Lab prediction.

There are many possible reasons for this difference, in particular, the size of the SPT plant, the different layouts used, the assumptions made in the calculations, the lack of specific information on key Gemasolar parameters, such as the receiver dimensions, the abovementioned problem with the precise definition of the tower optical height, the actual reflectivity of Sener heliostats and the cleanliness considered, TMY data used, etc.

However, this discrepancy may be considered reasonable because it is of the order of magnitude of the differences between the Sun-Lab and Sargent and Lundy predictions.

Finally, Figs. 7 and 8 review how the annual collector efficiency or field efficiency varies with the receiver radius (a receiver height $HR=2RR+1$ has been assumed for all the cases) and the tower optical height, respectively. The layout used in such calculations has been the optimum given by Fig. 5a. The other data for each figure is the reference case in Table 1.

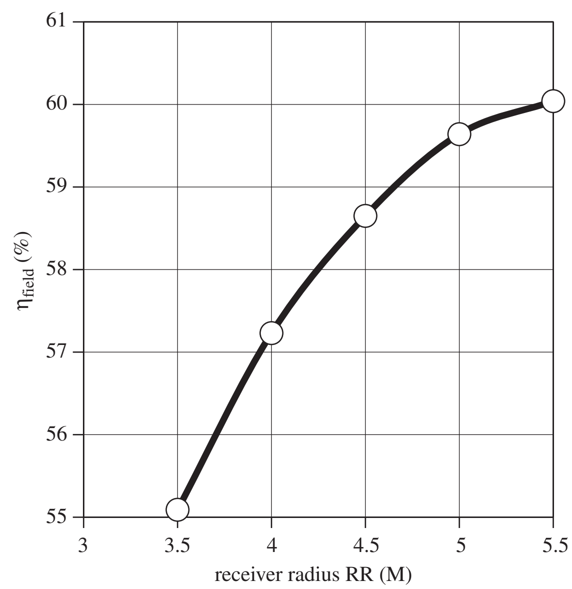


Fig. 7. Field efficiency vs. receiver radius for optimum layout (Fig. 5a). THT=130 m.

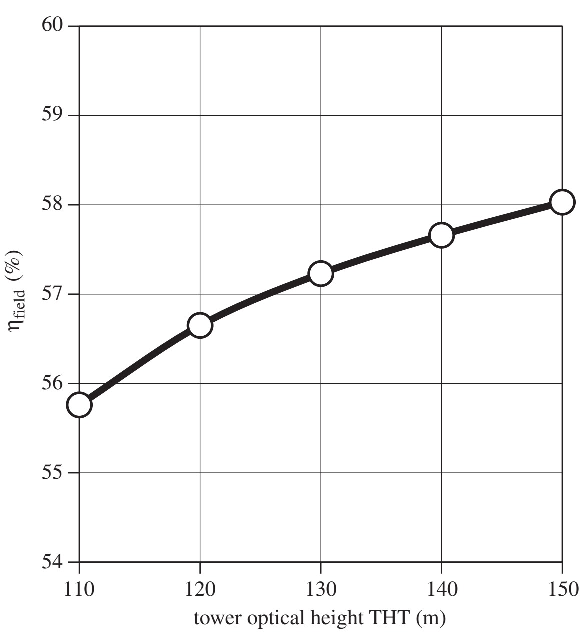


Fig. 8. Field efficiency vs. tower optical height for optimum layout (Fig. 5a). $RR=4$ m.

These figures should also be taken with care because the optimum field efficiencies certainly would change with the input parameters used, in particular with the tower height due its close relation with blocking. Furthermore, the slope and tracking errors of Sener heliostats is obviously a key parameter too and the information found on them has been rather limited [37].

With these caveats in mind, Fig. 7 shows that the annual collector efficiency of 56% suggested in the Sargent and Lundy study would correspond here with a receiver radius of about 3.75 m, whilst in this study it has been set to 4 m (see Table 1 with the reference values used). On the other hand, Fig. 8 clearly shows that the annual collector efficiency discrepancies with the Sargent and Lundy study cannot be due to the tower optical height, i.e., the tower should be much lower than that of the Gemasolar plant (with a receiver radius of 4 m) to obtain 56%.

Finally, in view of Figs. 7 and 8, the receiver dimension would seem a much more influential parameter than the tower height, although again it is necessary to notice that the optimized layouts and their efficiencies could be modified working with other heights. Furthermore, the receiver dimensions are closely related to thermal losses [16–18,38,46–48], which have not been addressed here.

8. Conclusions

In this review, it is clearly shown that, in spite of the higher thermodynamic efficiency (due to higher temperatures in a central receiver) reached by SPT systems, the complex optimized design of heliostat fields and the technical difficulties associated with expensive central receivers and scale-up problems have led to some delay in the full establishment of tower systems with respect to parabolic trough systems. A major expansion of PT systems in USA and Spain has been occurring in recent years due to their reliability, modularity and much less complex design.

SPT systems are gradually being highly promoted, mainly in USA, where SPT systems larger than 300 MWe are expected in the next few years provided that economic incentives are maintained. However, several years of reliable operation of PT systems have also proven the convenience of their scale-up to bigger powers (>300 MWe), also in USA. In conclusion, the battlefield between solar power tower centrals and parabolic trough systems has moved from Spain to USA. Furthermore, the very recent changes in Spanish government regulations (2012) on renewable power generation could complicate the status and near future of SPT and PT systems in Spain even more.

There are clear needs, therefore, for new tools to optimize the design of heliostat fields in SPT plants given the huge boost in power and number of units that these systems will experience in future years.

Nevertheless, a recent review by the authors [14] shows that the reported codes do not give enough details about a complex and key task inside the full general optimization process, namely how to optimally locate thousands of heliostats in the field each time the set of input parameters is changed seeking a minimum capital cost-annual energy ratio for the plant.

Focusing on the problem, this work addresses this task in depth with the help of a new code partially presented elsewhere [14], called *campo*, whose major feature is the ability to perform fast and accurate calculations of the shadowing and blocking factor for each and every one of the heliostats in the field for radial staggered layouts not only for a specific layout, but also

during the optimization task process when the layout is also changing.

The key idea of this optimization task is the well-known [15–17] shadowing and blocking factor and the other optical factor trade-off, i.e., *campo* proceeds from the densest field with the worst f_{sb} but the best values for the other optical factors towards gradually expanded fields. The maximum energy collected (indeed the maximum values of the field average annual averaged optical efficiency, in short η_{field}) or the stop of the radial-only expansion process is clearly found when this η_{field} begins to decline.

Taking as a reference case the scarce published data [7,34–38] on Gemasolar, the first solar thermal tower commercial plant (20 MWe) with molten salt storage in the world, this well-known trade-off has been put into practice using the *campo* code to confirm its validity as a reliable method of arranging thousands of heliostats efficiently in the field.

In the radial staggered layout used by *campo*, the field is naturally divided in zones. Taking into consideration such zones during this search for the optimum expanded layout, it would seem that each zone has its own maximum expansion. These zone maximums are reached when their gradual expansions start to move the other outer zones into far locations (from the tower) with worse optical efficiencies thus just dropping the whole η_{field} in spite of such expansions actually improving partial efficiency in the original zone.

Furthermore, it has been found that the optimization should proceed zone by zone from the inner to the outer zones, thus establishing a clear gradual and easily reproducible optimization. Fig. 6 gives a graphical overview of how *campo* works.

For the input parameters shown in Table 1 the maximum field efficiency reached is in the narrow range of 57.234–57.238%. These results should be taken with extreme care due the limited information about Gemasolar in Table 1, in which many key parameters have been assumed.

The first maximum efficiency found corresponds to constant radial increments for each zone, namely maximum density in the first zone $\Delta R_1 = \cos 30^\circ \cdot \mathrm{DM}$, DM = 15.7 m being the diagonal of the whole Sener heliostat used in Gemasolar. In zone 2 $\Delta R_2 = 1.4\mathrm{DM}$, and the larger radial increment in zone 3 (the outer zone) $\Delta R_3 = 2\mathrm{DM}$.

The second optimum value has been found growing linearly the radial distance between consecutive rows in zones 2 and 3, although each zone has its own expression, which matches the former optimum increments at the end of each zone. Therefore, based on limited experience with this new procedure, it is not immediately clear whether linear variations in the radial distance between consecutive rows over constant increments in each zone are an advantage.

The maximums found have been very flat, which is in agreement with the former experience of the first studies on this type of plant [15–17].

Using a deformed drawing of the Gemasolar layout as a limited source of information [37] (so these comments should be taken with extreme care), it has been seen that the arrangement of heliostats in Gemasolar is rather different from that proposed here. In the outer zones of Gemasolar, priority would have been given to the azimuth distance between adjacent heliostats, thus lowering the radial distances in an effort to reduce receiver dimensions.

However, as the number of heliostats per row is a direct function of the azimuth distance, the larger the azimuth distance, the lower the number of heliostats per row. With a fixed number of heliostats, this would mean more rows and finally longer distances. Indeed, the longest distance both in Gemasolar and *campo* are quite similar.

As is well known [15–18], the receiver dimensions would appear to be a much more influential parameter on annual efficiency than tower height, although this should be taken with caution because the tower height variations checked here have used the previous optimized radial distances between rows.

Highlight that the procedure successfully checked here for optimization layouts of solar power tower systems is actually independent of the code. Any code with the ability to calculate the time variations of Eq. (1) accurately, as some of those reviewed here, may include it without any problems. Even this procedure is not strictly limited to radial staggered layouts: we simply would start from the densest possible layouts progressing towards expanded fields (in which the relative distances between heliostats increase). The development of annual performance with the expansion would mark the end of the process.

Finally, comment that the optimization layout for a specific set of input parameters, as that presented here for Table 1 data, should be repeated for different values of the key parameters seeking for the minimum cost-annual energy ratio. Given the lack of open accurate capital cost data about key elements of the collector field, it would be interesting to find simplified procedures, mainly based on annual energy, to establish optimum values of receiver dimensions and tower height for a fixed number of heliostats.

In [47], it was already suggested using the intercept-thermal losses trade-off to establish the dimensions of the receiver. So that thermal losses models [47–48] of the receiver have to be included in the procedure. Work is in progress.

Acknowledgments

The authors want to thank the Spanish Minister of Science and Innovation (MICINN) for the funding of this research through the research project ENE2009-10268.

References

[1] Sargent, Lundy. Assessment of parabolic trough and power tower solar technology cost and performance forecast (final). Chicago: SL-5641; 2003.
[2] DLR. European concentrated solar thermal road-mapping (ECOSTAR). EU-funded study SES6-CT-2003-502578; 2005.
[3] Li J. Scaling up concentrating solar thermal technology in China. Renewable and Sustainable Energy Reviews 2009;13:2051–60.
[4] Ummadisingu A, Soni MS. Concentrating solar power-technology, potential and policy in India. Renewable and Sustainable Energy Reviews 2011;15: 5169–75.
[5] Pavlovic TM, Radonjic I, Milosvljevic DD, Pantic LS. A review of concentrating solar power plants in the world and their potential use in Serbia. Renewable and Sustainable Energy Reviews 2012;16:3891–902.
[6] Fernández-García A, Zarza E, Valenzuela L, Pérez M. Parabolic-trough solar collectors and their applications. Renewable and Sustainable Energy Reviews 2010;14:1695–721.
[7] Burgaleta JI, Arias S, Ramírez D. Gemasolar, the first tower thermosolar commercial plant with molten salt storage, In: SolarPACES, Granada, Spain, 20–23 September; 2011.
[8] Gould Jr. WR. Solarreserve's 565 MWt molten salt power towers, In: SolarPACES, Granada, Spain, 20–23 September; 2011.
[9] 〈http://www.csptoday.com〉.
[10] DOE. Basic research needs for solar energy utilization. Report on the basic energy sciences workshop on solar energy utilization, Washington; 2005.
[11] Kolb GJ, Jones SA, Donelly, MW, Gorman D, Thomas R, Davenport R et al. Heliostat cost reduction study. SAND2007-3293; 2007.
[12] Pacheco JE, Reilly HE, Kolb GJ, Tyner CE. Summary of the solar two: test and evaluation program. SAND2000-0372C; 2000.
[13] Collado FJ. Preliminary design of surrounding heliostat fields. Renewable Energy 2009;34:1359–63.
[14] Collado FJ, Guallar J. Campo: generation of regular heliostat fields. Renewable Energy 2012;46:49–59.
[15] Lipps FW, Vant-Hull LL. Shading and blocking geometry for a solar tower concentrator with rectangular mirror. ASME Paper 74-WA/Sol-11; 1974.
[16] Lipps FW, Vant-Hull LL. A cellwise method for solar central receivers systems. Solar Energy 1978;20:505–16.
[17] Lipps FW. Theory of cellwise optimization for solar central receivers. SAND85-8177; 1985.

[18] Kistler BL. A user's manual for DELSOL3: a computer code for calculating the optical performance and optimal system design for solar thermal central receiver plants. SAND86-8018; 1986.
[19] Schmitz M, Schwarzbölz P, Buck P, Pitz-Paal R. Assessment of the potential improvement due to multiple apertures in central receiver systems with secondary concentrators. Solar Energy 2006;80:111–20.
[20] Schwarzbölz P, Schmitz M, Pitz-Paal R. Visual HFLCAL—a software tool for layout and optimization of heliostat fields, In: SolarPACES, Berlin, Germany. 15-18 September; 2009.
[21] Garcia P, Ferriere A, Bezian J. Codes for solar flux calculation dedicated to central receiver system applications: a comparative review. Solar Energy 2008;82:189–97.
[22] Leary P, Hawkins J. A user guide for MIRVAL computer code for comparing designs of heliostat receiver optics for central receiver solar power plants. SAND82-0181; 1979.
[23] Wendelin T. SolTRACE: a new optical modelling tool for concentrating solar optics, In: proceedings of the ISEC 2003: international solar energy conference, 15–18 March 2003. Kohala Coast, Hawaii, NY: American Society of Mechanical Engineers; 2003. pp. 253–260.
[24] 〈http://www.nrel.gov/csp/soltrace/download.html〉.
[25] Sánchez M, Romero M. Methodology for generation of heliostat field layout in central receiver systems based on yearly normalized energy surfaces. Solar Energy 2006;80:861–74.
[26] Yao Z, Wang Z, Lu Z, Wei X. Modeling and simulation of the pioneer 1 MW solar thermal central receiver system in China. Renewable Energy 2009;34: 2437–46.
[27] Wei X, Lu Z, Wang Z, Yu W, Zhang H, Yao Z. A new method for the design of the heliostat field layout for solar tower power plant. Renewable Energy 2010;35:1970–5.
[28] Leonardi E, D'Aguanno B. CRS4-2: a numerical code for the calculation of the solar power collected in a central receiver system. Energy 2011;36:4828–37.
[29] Noone CJ, Torrilhon M, Mitsos A. Heliostat field optimization: a new computationally efficient model and biomimetic layout. Solar Energy 2012;86:792–803.
[30] Meinecke W. IAS-RL-100200-028, Almería, Spain; 1982.
[31] Schwarzbölz P, Harz T, Hennecke K, Hoffschmidt B, Koll G, Shchmitz M. The solar tower Jülich—a research and demonstration plant for central receiver systems, In: SolarPACES, Berlin, Germany, 15–18 September; 2009.
[32] 〈http://www.psa.es/webeng/index.php〉.
[33] 〈http://abengoasolar.com/web/en/index.html〉.
[34] Relloso S, Lata J. Molten salt thermal storage: a proven solution to increase plant dispatchability. Experience in Gemasolar tower plant, In: SolarPACES, Granada, Spain, 20–23 September; 2011.
[35] Ortega JI, Burgaleta JI, Téllez FM. Central receiver system (CRS) solar power plant using molten salt as heat transfer fluid, In: SolarPACES, Sevilla, Spain, 20–24 June; 2006.
[36] Vázquez J, Relloso S, Domingo M, Valverde A, Monterreal R, García G. Sener heliostat design and testing, In: SolarPACES, Sevilla, Spain, 20–24 June; 2006.
[37] Lata J, Alcalde S, Fernández D, Lecube X. First surrounding field of heliostats in the world for commercial solar power plants—Gemasolar, In; SolarPACES, Perpignan, France, 21–24 September; 2010.
[38] Lata J, Rodríguez M, Álvarez de Lara M. High flux central receivers of molten salts for the new generation of commercial stand-alone solar power plants, In: SolarPACES, Sevilla, Spain, 20–24 June ; 2006.
[39] Collado FJ. One-point fitting of the flux density produced by a heliostat. Solar Energy 2010;84:673–84.
[40] Collado FJ, Gómez A, Turégano JA. An analytic function for the flux density due to sunlight reflected from a heliostat. Solar Energy 1986;37:215–34.
[41] Guo M, Wang Z. On the analysis of an elliptical Gaussian flux image and its equivalent circular Gaussian flux images. Solar Energy 2011;85:144–1163.
[42] Collado FJ, Guallar J. Design of solar tower plants heliostat by heliostat: the blocking factor, In: SolarPACES, Berlin, Germany, 15–18 September; 2009.
[43] Collado FJ. Design of solar tower plants heliostat by heliostat: the shadowing and blocking factor, In; SolarPACES, Granada, Spain, 20–23 September; 2011.
[44] Sassi G. Some notes on shadow and blockage effects. Solar Energy 1983;31: 331–3.
[45] Collado FJ, Turégano JA. Calculation of the annual thermal energy supplied by a defined heliostat field. Solar Energy 1989;42:149–65.
[46] Martín JC. Solar Tres: first commercial molten salt central receiver plant, In: NREL CSP technology workshop, Denver, USA, March 7; 2007.
[47] Pitman CL, Vant-Hull LL. Receiver loss study; optics of optimized solar central receiver systems as a function of receiver thermal loss per unit area. SAND85-8176; 1985.
[48] Boehm RF. Review of thermal losses of solar central receivers. SAND85-8019; 1986.